Preparing attosecond coherences by strong-field ionization

Stefan Pabst,[1,2] Manfred Lein,[3] and Hans Jakob Wörner[4]

[1]*Center for Free-Electron Laser Science, DESY, Notkestrasse 85, 22607 Hamburg, Germany*

[2]*ITAMP, Harvard-Smithsonian Center for Astrophysics, 60 Garden Street, Cambridge, Massachusetts 02138, USA*

[3]*Institut für Theoretische Physik and Centre for Quantum Engineering and Space-Time Research (QUEST), Leibniz Universität Hannover, Appelstraße 2, 30167 Hannover, Germany*

[4]*Laboratorium für Physikalische Chemie, ETH Zürich, Vladimir-Prelog-Weg 2, 8093 Zürich, Switzerland*

(Received 6 October 2015; published 11 February 2016)

Strong-field ionization (SFI) has been shown to prepare wave packets with few-femtosecond periods. Here, we explore whether this technique can be extended to the attosecond time scale. We introduce an intuitive model, which is based on the Fourier transform of the subcycle SFI rate, for predicting the bandwidth of ionic states that can be coherently prepared by SFI. The coherent bandwidth decreases considerably with increasing central wavelength of the ionizing pulse but it is much less sensitive to its intensity. Many-body calculations based on time-dependent configuration-interaction singles support these results. The influence of channel interactions and laser-induced dynamics within the ion is discussed. Our results further predict that multicycle femtosecond pulses can coherently prepare subfemtosecond wave packets with higher selectivity and versatility compared to single-cycle pulses with an additional sensitivity to the mutual parity of the prepared states.

DOI: 10.1103/PhysRevA.93.023412

I. INTRODUCTION

The measurement of electronic wave packets has recently attracted widespread interest. Time-domain studies of electrons in atoms, molecules, and the condensed phase offer new approaches to understanding electronic structure and electronic correlations (see, e.g., [1–6]). Electronic wave packets have been measured in the valence shell of atomic ions using transient absorption [7,8] or sequential double ionization [9,10] and in the valence shell of neutral molecules using high-harmonic spectroscopy [11–13].

One necessary condition for creating electronic motion is the population of multiple electronic states. Strong-field ionization is well known to fulfill this condition [14–18]. The second requirement, which has received much less attention, is the coherent preparation of these electronic states. Since ionization is inherently an open-system quantum process with respect to the cation, the coherence between the quantum states of the cation is always imperfect. In other words, strong-field ionization (SFI) leaves the ion in a mixed state which may display no time dependence at all. Hence, a method for predicting the degree of coherence created by SFI is urgently needed.

The partial coherence of electronic states generated by SFI has been studied in rare-gas ions, both theoretically [19,20] and experimentally [7,8]. These studies showed that the degree of coherence decreases with increasing duration of the ionizing pulse and suggested that the optical cycle sets a natural lower bound to the period of wave packets accessible through SFI.

The subject of this article is particularly relevant for applying SFI to initiate charge migration [1,21,22] which is usually discussed in the context of single-photon ionization in the sudden limit. A recent study of single-photon ionization by attosecond pulses has shown that a necessary condition for the coherent population of cationic states is that the bandwidth of the ionizing radiation exceeds their energetic separation [23]. In contrast, the existence of a similar condition for SFI in the nonperturbative regime is not obvious and has not, to our knowledge, been discussed previously. In the case of perturbative, nonresonant SFI by n photons, the coherence bandwidth should be given by the Fourier transform of the nth power of the time-dependent electric field. This pronounced dependence on the number of photons should disappear in the nonperturbative regime. Alternatively, in analogy to single-photon ionization, the spectral width of the created photoelectron wave packet (two times the ponderomotive potential) could be the key quantity in determining the coherence. We show that it is in fact a third quantity, namely, the temporal confinement of SFI, that is the key to defining the coherent bandwidth. This result suggests a surprisingly simple and general method for predicting the potential of SFI to prepare attosecond dynamics in a specific system.

In this article, we introduce the concept of a "coherence window" which represents the bandwidth of ionic states that can be coherently prepared by SFI. The coherence window is obtained by Fourier transforming the subcycle time dependence of the SFI rate. We derive this conceptually intuitive model from the strong-field approximation (SFA) and validate it using the time-dependent configuration-interaction singles (TDCIS) method [24,25], an *ab initio* many-body approach. Our model predicts a pronounced decrease of the coherence window with increasing central wavelength. The TDCIS results reveal substantial changes in the presence of laser-driven transitions in the ion and a reduction of the coherence caused by channel interactions. Most importantly, all results agree in displaying energy-domain recurrences of the coherence that enable highly coherent attosecond wave packets to be selectively prepared by multicycle femtosecond pulses. This property is particularly valuable for preparing only selected electronic coherences in molecules where SFI would usually prepare highly complex wave packets.

II. RESULTS

A. Simple model

Our approach is motivated by the Fourier principle. The more a physical event is confined in time, the larger is the

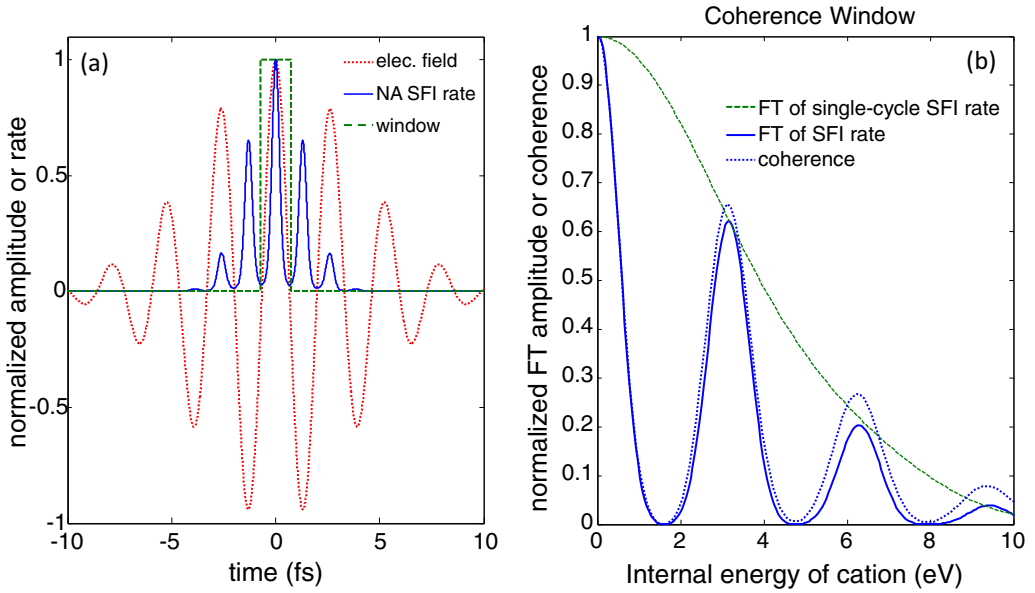

FIG. 1. (a) Electric field of a 6.3 fs pulse centered at 800 nm and nonadiabatic SFI rate for a peak intensity of 10^{14} W/cm^2, ionization energy of 12.1 eV, and angular momentum quantum numbers $\ell = 1$ and $m = 0$. (b) Fourier-transform amplitude of the full SFI rate (solid blue line) or the SFI rate restricted to the window shown in (a) (green dashed line). The dotted blue line shows the degree of coherence C between the ground state and an excited state with $I_p = 12.1$ eV $+ \Delta E$ as a function of ΔE, calculated according to Eqs. (3) and (4).

associated energy bandwidth. Applied to SFI, we conjecture that the subcycle evolution of the strong-field ionization rate $\Gamma(t) := \Gamma[\mathcal{E}(t)]$ is the key quantity in determining the bandwidth of states that can be coherently prepared, where $\mathcal{E}(t)$ is the instantaneous electric-field strength. The highly nonlinear dependence of Γ on $\mathcal{E}$ results in a wide coherence window that can span several electron volts. We first illustrate this result numerically, then derive it from the SFA and finally test it against *ab initio* multielectron (TDCIS) calculations.

Figure 1(a) shows a linearly polarized few-cycle pulse and the associated nonadiabatic SFI rate [26] for a hydrogen-like atom. Figure 1(b) shows the absolute value of the Fourier transform of both the complete SFI rate (full blue line) and its restriction to the central half cycle (green dashed line). This latter curve represents the coherence window associated with a single half cycle, whereas the former represents the coherence window associated with the complete pulse.

The following conclusions can be drawn from Fig. 1, which shows results for 800 nm central wavelength and 10^{14} W/cm^2 peak intensity. These pulse parameters give rise to a half width at half maximum of 3.9 eV, corresponding to a temporal period of 1.06 fs. The shortest accessible period thus lies far below the optical-cycle period of 2.67 fs, which is a consequence of the nonlinearity of SFI. A single-cycle pulse can thus coherently prepare any pair of levels lying within the single-cycle coherence window [dashed green line in Fig. 1(b)], whereas a multicycle pulse can only coherently prepare levels lying within the narrower maxima of the multicycle coherence window (full blue line). In the case of an inversion symmetric medium these maxima are spaced by $2n\omega$ (with n integer) because the SFI rate does not distinguish between positive and negative extrema of the electric field and thus possesses twice the angular frequency ω of the electric field. The case of non-inversion-symmetric systems and the role of parity are discussed below.

B. Derivation from the strong-field approximation

We now provide an analytical derivation of the coherence window from the SFA. The SFA [27–32] has been widely used to calculate photoelectron momentum distributions. It has explained properties of SFI such as above-threshold ionization peaks and their ponderomotive shift, intracycle interference [33,34], and the lateral width of momentum distributions [35]. The SFA has not previously been used to investigate coherence in ions. Here we use the SFA to derive the density matrix of ions created by SFI. An atom or a molecule, initially in its ground state Ψ_0, is ionized by a linearly polarized pulse with electric field $\mathcal{E}(t)\mathbf{e}_z$. In length-gauge SFA, the complex amplitude for creating an ion in the state J accompanied by an electron with momentum $\mathbf{k}$, taken at the final time t_f and in atomic units, is

$$M_J(\mathbf{k}) = i \int_{-\infty}^{t_f} dt\, D_J(\mathbf{v}_\mathbf{k}(t))\mathcal{E}(t) e^{iS_J(\mathbf{k},t)} e^{-iE_J t_f}. \qquad (1)$$

Here $D_J(\mathbf{v}) = \langle \mathbf{v}, J | D_z | \Psi_0 \rangle$ is the transition dipole to the product state $|\mathbf{v}, J\rangle$ of a plane wave with momentum $\mathbf{v}$ and the ionic state J with energy E_J relative to the neutral-atom ground state. The electron kinetic momentum is $\mathbf{v}_\mathbf{k}(t) = \mathbf{k} + \mathbf{A}(t)$ with $\mathbf{A}(t) = A(t)\mathbf{e}_z = -\int^t \mathcal{E}(t')\mathbf{e}_z\, dt'$, and the action is given by $S_J(\mathbf{k},t) = E_J t - \frac{1}{2}\int_t^{t_f} \mathbf{v}_\mathbf{k}(t')^2\, dt'$.

Tracing out the degrees of freedom of the unobserved photoelectron produces the reduced density matrix of the ion,

$$\rho_{JK} = \int d^3k\, M_J(\mathbf{k}) M_K(\mathbf{k})^*. \qquad (2)$$

We evaluate the time integral in Eq. (1) by a saddle-point approximation. In the tunneling regime, the complex saddle-

point times given by $\frac{\partial}{\partial t} S_J(\mathbf{k},t) = 0$ are near the classical ionization times defined by $k_z + A(t) = 0$. For simplicity, we assume that the transition dipoles do not have a singularity at the saddle point, which is true for bound states of limited spatial extension. Electron wave packets contributing to the same final momentum, but emitted at different times, have small overlap because of rapid wave-packet spreading in the continuum. Hence, we determine the coherence by neglecting terms where two ionic states are populated at different classical times. We restrict the k_z integration to the classically allowed range and rewrite it as a time integral by substitution. For $t_f \to \infty$, small E_J and small $k_\perp^2 = k_x^2 + k_y^2$, we thus find

$$\rho_{JK} = \int_{-\infty}^{\infty} dt \sqrt{\Gamma_J \Gamma_K}\, \mathrm{sgn}[\mathcal{E}(t)]^{(2-P_J-P_K)/2} e^{i(E_J - E_K)t}. \quad (3)$$

To reach this result, we have approximated $D_J = c_J\, D(k_\perp) f_J(\mathrm{sgn}[\mathcal{E}(t)])$ with a constant c_J and a state-independent function D. The function $f_J(x) = x^{(1-P_J)/2} |f_J(x)|$ with $P_J = \pm 1$ describes inversion symmetry: for states with defined electronic parity, we have $f_J(x) = x^{(1-P_J)/2}$; for polar molecules, f_J accounts for the asymmetry of ionization. The instantaneous ionization rate is given by $\Gamma_J(t) = \exp(-\frac{2\sqrt{2E_J}^3}{3|\mathcal{E}(t)|}) |c_J\, f_J|^2\, \Gamma_\perp(t)$ with $\Gamma_\perp(t)$ capturing the state-independent integral over the transverse momentum. The ionization rates can be quantitatively calculated by improved methods that include the Coulomb potential, nonadiabatic effects, or molecular electronic structure [26,31,36,37]. These results enable us to calculate the coherence between states J and K as follows:

$$C = \frac{|\rho_{JK}|}{\sqrt{\rho_{JJ}\rho_{KK}}}. \quad (4)$$

The limit $C = 1$ represents a pure state, whereas $C = 0$ represents a mixed state which displays no time dependence at all.

The results obtained from this derivation are compared to the simple model in Fig. 1. The dotted curve in Fig. 1 shows the degree of coherence C between the ground state and an excited state as a function of their energy separation, calculated according to Eqs. (3) and (4) using the nonadiabatic tunneling rate [26]. The close agreement between the two blue curves in Fig. 1 shows that the Fourier-transform-based coherence window (full curve) is a good predictor of the coherence (dotted curve) derived from the SFA. These results thus confirm our conjecture and Eq. (3) simultaneously introduces two important refinements. First, the coherence window depends on the SFI rates to both final states, the ground and the excited state. Indeed, Eq. (3) represents the Fourier transform of the geometric mean of the two ionization rates evaluated at the difference of the ionization energies $\Delta E = E_K - E_J$. The comparison of the full and dotted lines in Fig. 1(b) shows that this effect is only important at high internal energies of the cation. Second, the shape of the coherence window is sensitive to the parity of the final states. If the states J and K have the same parity ($P_J P_K = 1$), the coherence will peak at $\Delta E = 0$. For a long pulse, the integrand is nearly a periodic function leading to peaks of the coherence when ΔE is an even multiple of ω. If, on the other hand, J and K differ in parity ($P_J P_K = -1$) the integrand changes sign every half cycle and the coherence peaks at odd multiples of ω. For polar molecules, electronic parity is not defined and, consequently, the coherence peaks appear at all integer multiples of ω.

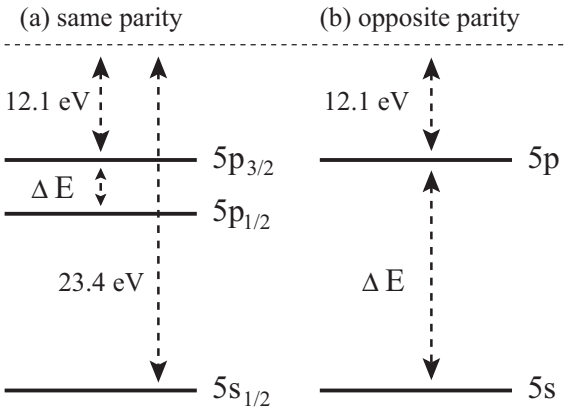

FIG. 2. Level structure of the artificial xenon atom used in the TDCIS calculations to represent the case of initial states of the (a) same parity and (b) opposite parities.

C. TDCIS calculations

We now validate these predictions beyond the framework of the SFA and additionally analyze the roles played by laser-induced transitions and channel interactions by turning to TDCIS calculations [38,39]. All TDCIS calculations in this article use an artificial Xe atom with tunable energy-level separations as illustrated in Fig. 2. Figure 3 illustrates the role of parity through the coherence C between two ionic states of (a) the same and (b) opposite parities as a function of their energy separation ΔE. The lowest ionization energy (12.1 eV) is kept constant in all cases. We illustrate the case of equal parity, using the $5p_{1/2}^{-1}$ and $5p_{3/2}^{-1}$ fine-structure states ($m_J = 1/2$) of Xe^+. The $5s^{-1}$ and $5p^{-1}$ states with spin-orbit coupling artificially set to zero serve as an illustration for the case of final states with opposite parities.

III. DISCUSSION

Figure 3 compares the TDCIS results (red line) with the model [Eq. (4)] based on the nonadiabatic tunneling rates. Both theories agree in predicting the local maxima of the coherence at $\Delta E = 2n\omega$ for the same-parity case and $\Delta E = (2n+1)\omega$ for the opposite-parity case. In the case of equal parities [Fig. 3(a)], a very good general agreement between the model and the TDCIS calculations is obtained. This result shows that the model accurately captures the physical processes behind the creation of coherence. In the case of opposite parities [Fig. 3(b)], the model and TDCIS calculations still agree very well, except for the 1ω peak which is unexpectedly small in the TDCIS calculations. Panel (c) shows that this suppression is a consequence of laser-driven transitions between the dipole-coupled $5p^{-1}$ and $5s^{-1}$ states of Xe^+. When the corresponding transition dipole moment is set to zero in the TDCIS calculations, the normal situation of monotonically decreasing coherence peaks is recovered.

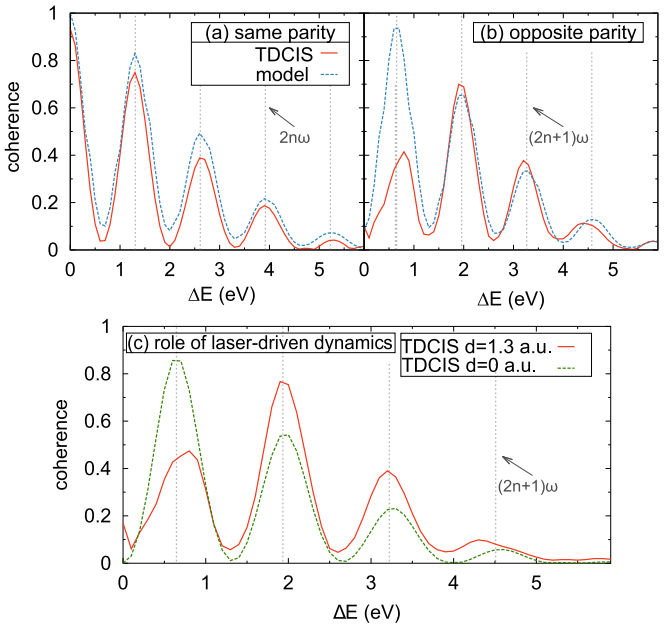

FIG. 3. Coherence between two ionic states prepared by SFI with the same (a) or opposite [(b),(c)] parities as a function of their separation ΔE. The states in (a) are the $5p_{1/2}^{-1}$ and $5p_{3/2}^{-1}$ of Xe^+ ($m_J = 1/2$), and in (b) the states $5s^{-1}$ and $5p_0^{-1}$ with spin-orbit interactions turned off. Results are shown for TDCIS (solid red) and Eq. (4) using nonadiabatic tunneling rates [26] (dotted blue). (c) same as (b) comparing the full TDCIS calculation with the result obtained by setting the $5s^{-1} \leftrightarrow 5p_0^{-1}$ transition dipole moment to zero. In all panels the ionizing pulse is 12.7 fs (FWHM) long, has a peak intensity of 10^{14} W/cm^2, and a central wavelength of 1900 nm. The vertical dashed lines mark energy splittings corresponding to $2n\omega$ and $(2n+1)\omega$, respectively.

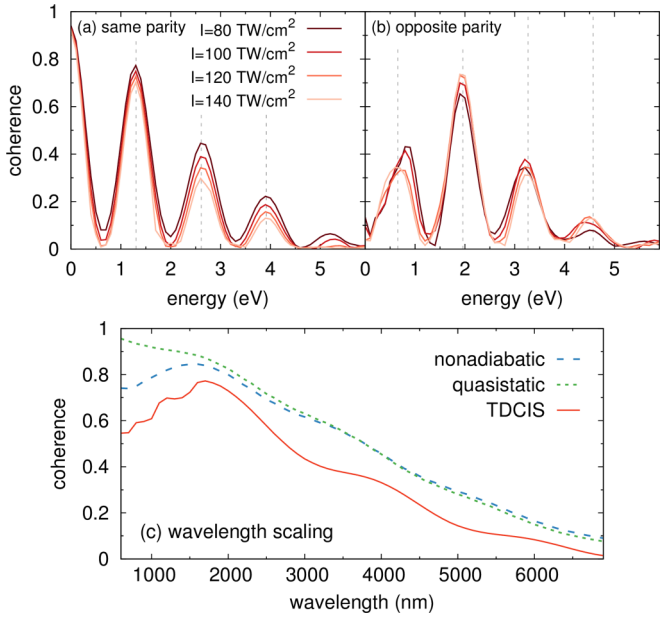

FIG. 4. (a) Effect of the intensity on the coherence between the $5p_{1/2}^{-1}$ and $5p_{3/2}^{-1}$ states of Xe^+ ($m_J = 1/2$) as a function of their energy separation from TDCIS calculations. (b) Same as (a) for the $5s^{-1}$ and $5p_0^{-1}$ states. All other pulse parameters are the same as in Fig. 3. (c) Effect of the wavelength on the coherence between $5p_{1/2}^{-1}$ and $5p_{3/2}^{-1}$ using an energy-level separation of 1.3 eV, a peak intensity of 10^{14} W/cm^2, and a single-cycle pulse at each wavelength.

Figure 4 shows the dependence of the coherence on the intensity [(a),(b)] and wavelength (c) of the driving pulse. The influence of the intensity is generally rather weak. In the case of equal parities (a), higher intensities suppress the coherence for high-lying excited states. This is explained by the broadening of the temporal ionization window with increasing intensity. In the case of opposite parities (b), an increase of the intensity leads to a suppression of the first peak, which supports the interpretation of Figs. 3(b) and 3(c) that laser-induced transitions reduce this coherence. A complementary behavior is observed in the 3ω peak which is found to increase with the intensity.

The effect of the wavelength is studied in Fig. 4(c) by displaying the coherence between the $5p_{1/2}^{-1}$ and $5p_{3/2}^{-1}$ states of Xe^+ ($m_J = 1/2$), using a single-cycle laser pulse at all wavelengths. We compare the results of the model using nonadiabatic tunneling rates (blue dashed line) with the model using quasistatic rates (green dotted line). We find that the two models agree at long wavelengths, but the quasistatic rates overestimate the coherence at wavelengths ranging from 800 to 2000 nm. The additional comparison with TDCIS calculations (red line) shows that the interaction between ionization channels, present in TDCIS but absent in both model calculations, additionally suppresses the degree of coherence at all wavelengths.

IV. CONCLUSION

In conclusion, we have introduced an intuitive approach to predicting the degree of coherence between multiple states of a cation prepared by SFI. We showed that laser-induced transitions, nonadiabatic effects in tunneling, and channel interactions generally tend to decrease the degree of coherence predicted by our simple model. We have further shown how coherent hole wave packets can be selectively created with multicycle strong-field pulses that may be much longer than the period of the prepared dynamics itself. This property alleviates the need for single-cycle IR pulses that are challenging to create. In inversion-symmetric systems, the hole coherence maximizes at $\Delta E = 2n\omega$, with n integer, for ionic states of the same parities and at $\Delta E = (2n+1)\omega$ for states of opposite parities. In systems lacking inversion symmetry, such as polar molecules, local maxima of the coherence are in contrast expected for $\Delta E = n\omega$. The described approach finally also offers a way to selectively create coherent wave packets involving specific hole states that could not be generated with short "delta-like" strong-field or attosecond XUV pulses. A generalization to multicolor pulses opens the path to an even higher selectivity in creating attosecond electronic wave packets involving multiple ionic states.

ACKNOWLEDGMENTS

S.P. is funded by the Alexander von Humboldt Foundation. This work was supported by the NSF through a grant to ITAMP. S.P. thanks the Helmholtz association for financial support through the Helmholtz Ph.D. prize. M.L. acknowl-

edges funding from the Deutsche Forschungsgemeinschaft. H.J.W. gratefully acknowledges funding from the European Research Council through an ERC starting grant (Contract No. 307270-ATTOSCOPE).

[1] L. Cederbaum and J. Zobeley, Chem. Phys. Lett. **307**, 205 (1999).
[2] J. Mauritsson, P. Johnsson, E. Mansten, M. Swoboda, T. Ruchon, A. L'Huillier, and K. J. Schafer, Phys. Rev. Lett. **100**, 073003 (2008).
[3] P. Eckle, A. N. Pfeiffer, C. Cirelli, A. Staudte, R. Dörner, H. G. Muller, M. Büttiker, and U. Keller, Science **322**, 1525 (2008).
[4] C. Ott, A. Kaldun, P. Raith, K. Meyer, M. Laux, J. Evers, C. H. Keitel, C. H. Greene, and T. Pfeifer, Science **340**, 716 (2013).
[5] M. Schultze, K. Ramasesha, C. Pemmaraju, S. Sato, D. Whitmore, A. Gandman, J. S. Prell, L. J. Borja, D. Prendergast, K. Yabana, D. M. Neumark, and S. R. Leone, Science **346**, 1348 (2014).
[6] C. Ott, A. Kaldun, L. Argenti, P. Raith, K. Meyer, M. Laux, Y. Zhang, A. Blattermann, S. Hagstotz, T. Ding, R. Heck, J. Madronero, F. Martin, and T. Pfeifer, Nature (London) **516**, 374 (2014).
[7] E. Goulielmakis, Z. Loh, A. Wirth, R. Santra, N. Rohringer, V. S. Yakovlev, S. Zherebtsov, T. Pfeifer, A. M. Azzeer, M. F. Kling, S. R. Leone, and F. Krausz, Nature (London) **466**, 739 (2010).
[8] A. Wirth, M. T. Hassan, I. Grguras, J. Gagnon, A. Moulet, T. T. Luu, S. Pabst, R. Santra, Z. A. Alahmed, A. M. Azzeer, V. S. Yakovlev, V. Pervak, F. Krausz, and E. Goulielmakis, Science **334**, 195 (2011).
[9] H. J. Wörner and P. B. Corkum, J. Phys. B **44**, 041001 (2011).
[10] A. Fleischer, H. J. Wörner, L. L. Arissian, L. R. Liu, M. M. Meckel, A. A. Rippert, R. Dörner, D. M. Villeneuve, P. B. Corkum, and A. Staudte, Phys. Rev. Lett. **107**, 113003 (2011).
[11] P. M. Kraus, S. B. Zhang, A. Gijsbertsen, R. R. Lucchese, N. Rohringer, and H. J. Wörner, Phys. Rev. Lett. **111**, 243005 (2013).
[12] D. Baykusheva, P. M. Kraus, S. B. Zhang, N. Rohringer, and H. J. Wörner, Faraday Discussions **171**, 113 (2014).
[13] S. B. Zhang, D. Baykusheva, P. M. Kraus, H. J. Wörner, and N. Rohringer, Phys. Rev. A **91**, 023421 (2015).
[14] G. N. Gibson, R. R. Freeman, and T. J. McIlrath, Phys. Rev. Lett. **67**, 1230 (1991).
[15] H. Akagi, L. Arissian, J. B. Bertrand, P. B. Corkum, M. Gertsvolf, D. Pavičić, D. M. Rayner, C. Smeenk, A. Staudte, D. M. Villeneuve, and H. J. Wörner, Laser Phys. **19**, 1697 (2009).
[16] S. Pabst, L. Greenman, D. A. Mazziotti, and R. Santra, Phys. Rev. A **85**, 023411 (2012).
[17] B. K. McFarland, J. P. Farrell, P. H. Bucksbaum, and M. Gühr, Science **322**, 1232 (2008).
[18] O. Smirnova, Y. Mairesse, S. Patchkovskii, N. Dudovich, D. Villeneuve, P. Corkum, and M. Y. Ivanov, Nature (London) **460**, 972 (2009).
[19] R. Santra, R. W. Dunford, and L. Young, Phys. Rev. A **74**, 043403 (2006).
[20] N. Rohringer and R. Santra, Phys. Rev. A **79**, 053402 (2009).
[21] J. Breidbach and L. S. Cederbaum, J. Chem. Phys. **118**, 3983 (2003).
[22] P. M. Kraus, B. Mignolet, D. Baykusheva, A. Rupenyan, L. Horný, E. F. Penka, G. Grassi, O. I. Tolstikhin, J. Schneider, F. Jensen, L. B. Madsen, A. D. Bandrauk, F. Remacle, and H. J. Wörner, Science **350**, 790 (2015).
[23] S. Pabst, L. Greenman, P. J. Ho, D. A. Mazziotti, and R. Santra, Phys. Rev. Lett. **106**, 053003 (2011).
[24] L. Greenman, P. J. Ho, S. Pabst, E. Kamarchik, D. A. Mazziotti, and R. Santra, Phys. Rev. A **82**, 023406 (2010).
[25] S. Pabst, Eur. Phys. J. Spec. Top. **221**, 1 (2013).
[26] G. L. Yudin and M. Y. Ivanov, Phys. Rev. A **64**, 013409 (2001).
[27] L. V. Keldysh, Zh. Eksp. Teor. Fiz. **47**, 1945 (1965) [Sov. Phys. JETP **20**, 1307 (1965)].
[28] F. H. M. Faisal, J. Phys. B **6**, L89 (1973).
[29] H. R. Reiss, Phys. Rev. A **22**, 1786 (1980).
[30] G. F. Gribakin and M. Y. Kuchiev, Phys. Rev. A **55**, 3760 (1997).
[31] V. S. Popov, Phys. Usp. **47**, 855 (2004).
[32] S. V. Popruzhenko, J. Phys. B **47**, 204001 (2014).
[33] F. Lindner, M. G. Schätzel, H. Walther, A. Baltuška, E. Goulielmakis, F. Krausz, D. B. Milošević, D. Bauer, W. Becker, and G. G. Paulus, Phys. Rev. Lett. **95**, 040401 (2005).
[34] T.-M. Yan and D. Bauer, Phys. Rev. A **86**, 053403 (2012).
[35] I. Dreissigacker and M. Lein, Chem. Phys. **414**, 69 (2013), attosecond spectroscopy.
[36] X. M. Tong, Z. X. Zhao, and C. D. Lin, Phys. Rev. A **66**, 033402 (2002).
[37] O. I. Tolstikhin, T. Morishita, and L. B. Madsen, Phys. Rev. A **84**, 053423 (2011).
[38] S. Pabst, L. Greenman, A. Karamatskou, Y.-J. Chen, A. Sytcheva, O. Geffert, and R. Santra, XCID program package for multichannel ionization dynamics, DESY, Hamburg, Germany, 2015, Rev. 1349.
[39] A pseudospectral grid with a radial box size of $130a_0$, 600 grid points, and a mapping parameter of $\zeta = 0.5$ are used. The complex absorbing potential starts at $100a_0$ and has a strength of $\eta = 0.002$. The maximum angular momentum is 15 and Hartree-Fock orbitals up to an energy of 10 a.u. are considered. The propagation method is Runge-Kutta 4 with a time step $dt = 0.05$ a.u. All $5s$ and $5p$ orbitals are active in the calculations.